Geophysical Research Letters

Supporting Information for

Multidecadal Intensification of Atlantic Tropical Instability Waves

Franz Philip Tuchen[1], Renellys C. Perez[1], Gregory R. Foltz[1], Peter Brandt[2,3], Rick Lumpkin[1]

[1] NOAA / Atlantic Oceanographic and Meteorological Laboratory, Miami, FL, USA

[2] GEOMAR Helmholtz Centre for Ocean Research Kiel, Kiel, Germany

[3] Faculty of Mathematics and Natural Sciences, Kiel University, Kiel, Germany

Corresponding author: Franz Philip Tuchen (franz.philip.tuchen@noaa.gov)

Contents of this file

- Text S1: Comparison of near-surface velocities from the drifter-wind-altimetry synthesis and moored velocity observations.

- Text S2: Covariance of zonal and meridional velocities from moored velocity observations at 0°, 23°W

- Figures S1 to S6

- Table S1

Text S1: Comparison of near-surface velocities from the drifter-wind-altimetry synthesis and moored velocity observations

Near-surface velocities are derived from a synthesis of in-situ drogued drifter velocity measurements, satellite winds, and altimetry-derived geostrophic velocity anomalies (*Lumpkin & Garzoli, 2011; Perez et al., 2019*) by simultaneously regressing the observed velocities, low-passed at 1.5 times the local inertial period with a floor of 1 day and a ceiling of 5 days, onto four spatially-varying, time invariant coefficients multiplying (a) the wind speed from the ERA-interim product (https://www.ecmwf.int/en/forecasts/datasets/reanalysis-datasets/era-interim) in the downwind and crosswind directions, and (b) the zonal and meridional geostrophic velocities derived from altimetry as provided by the Copernicus Marine and Environment Monitoring Service (CMEMS). These coefficients are then used to generate gridded, daily near-surface velocities from the same satellite products. We note that Ekman dynamics are not explicitly assumed, while CMEMS near-equatorial currents are derived from SLA using an algorithm derived from *Lagerloef et al. (1999)*. To address the reliability of near-surface velocities provided by this drifter-wind-altimetry synthesis, we compare this data set with velocity observations from current meters attached to the PIRATA moored surface buoys at 4°N, 23°W and at 0°, 23°W, both installed at 10 m depth (*Bourlès et al., 2019; Foltz et al., 2019*). In addition, we use current velocities from moored acoustic Doppler current profiler (ADCP) measurements from a subsurface mooring at 0°, 23°W (*Tuchen et al., 2022b*). Here, we are using ADCP data at the shallowest resolved depth at 20 m. Lastly, surface velocities from another current analysis product, the Ocean Surface Current Analyses Real-time (OSCAR) project, are used for comparison.

In Figure S1, horizontal current velocities are shown for one year in which all data sets provided data (Fig. S1a-d). Overall, we find good agreement of zonal and meridional velocities at 4°N, 23°W between the available data products (PIRATA, drifter-wind-altimetry synthesis, and OSCAR). OSCAR is provided at a 5-daily temporal resolution, whereas PIRATA current meter data is generally provided with hourly resolution and is then subsampled to 12-hour means (Fig. S1c-d). For this reason, some differences relative OSCAR and the drifter-wind-altimetry synthesis can be expected. The comparison shows that the occurrence of Tropical Instability Waves is reproduced by the products, but underestimates the large meridional velocity amplitudes and eddy kinetic energy associated with the waves (Fig. S1f). The correlation coefficients between PIRATA current velocities at 10 m depth and near-surface velocities at an approximate depth of 15 m from the drifter-wind-altimetry synthesis (using all available data between 2005-2022) are 0.46 for zonal and 0.60 for meridional velocities (Tab. S1). Correlations are slightly smaller between the PIRATA velocities and OSCAR, 0.50 for zonal and 0.56 for meridional velocity.

The same comparison was carried out at 0°, 23°W (Fig. S1a-b,e). The agreement between observed current velocities and those provided by the two data products is considerably lower on the equator. The correlation coefficients between PIRATA current velocities at 10 m depth and near-surface velocities at 15 m depth from the drifter-wind-altimetry synthesis (using all available data between 2005-2022) are 0.21 for zonal and 0.23 for meridional velocities (Tab. S1). The correlation coefficients between moored ADCP current velocities at 20 m depth and current velocities at 15 m depth from the drifter-wind-altimetry synthesis are 0.32 for zonal and 0.18 for meridional velocities. Although the corresponding correlations are slightly larger between the moored and OSCAR velocity estimates at 0°, 23°W, the correlations are still weaker than those found at 4°N, 23°W.

All correlation coefficients at 0°, 23°W and 4°N, 23°W shown in Tab. S1 are only slightly increased if a 5-day running mean is applied to the PIRATA, moored ADCP and drifter-wind-altimetry time series in order to adjust to the lower temporal resolution of OSCAR.

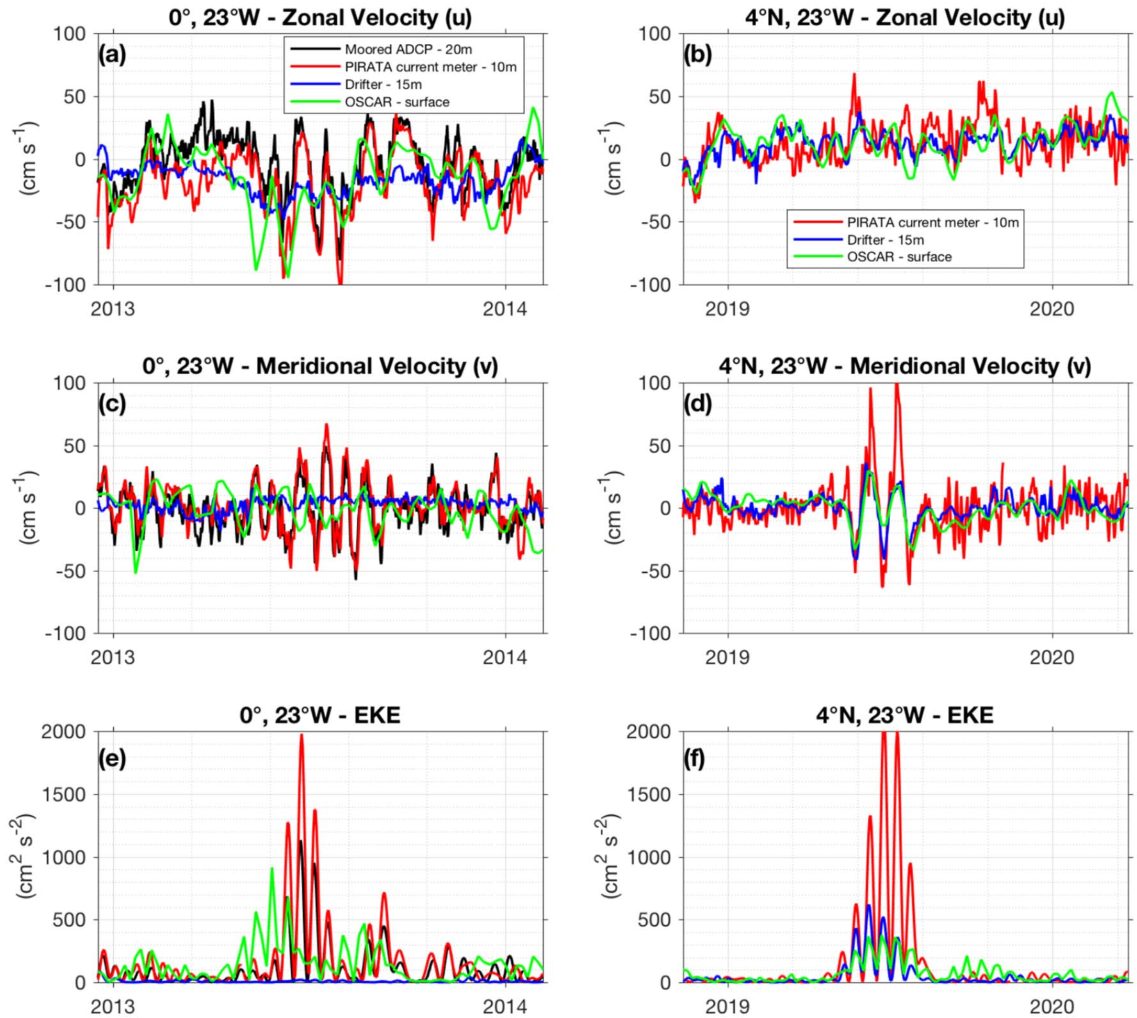

Figure S1. Time series of (a-d) zonal ($\boldsymbol{u}$) and meridional ($\boldsymbol{v}$) velocity and (e-f) eddy kinetic energy (EKE; $(\boldsymbol{u}'^2 + \boldsymbol{v}'^2)/\mathbf{2}$) at 0°, 23°W (left panels) and at 4°N, 23°W (right panels). Included are data from PIRATA current meter observations at 10 m (red), near-surface velocities from the drifter-wind-altimetry synthesis at an approximate depth of 15 m (blue), surface velocities from OSCAR (green), and at 0°, 23°W moored ADCP observations at 20 m (black). For both mooring sites, one year is chosen for which all products provided complete records: 2013 at 0°, 23°W and 2019 at 4°N, 23°W.

Correlation (u/v)	PIRATA	Moored ADCP	Drifter-altimetry	OSCAR
PIRATA	X	0.83 / 0.83	0.21 / 0.23	0.37 / 0.20
Moored ADCP		X	0.32 / 0.18	0.40 / 0.22
Drifter-altimetry	0.46 / 0.60		X	0.60 / 0.16
OSCAR	0.50 / 0.56		0.72 / 0.77	X

Table S1. Correlation coefficients for zonal ($\boldsymbol{u}$) and meridional ($\boldsymbol{v}$) velocity time series at 0°, 23°W (green shaded values) and at 4°N, 23°W (yellow shaded values) using all available data between 2005-2022 at both mooring sites. Note that long-term moored ADCP observations are only available at 0°, 23°W.

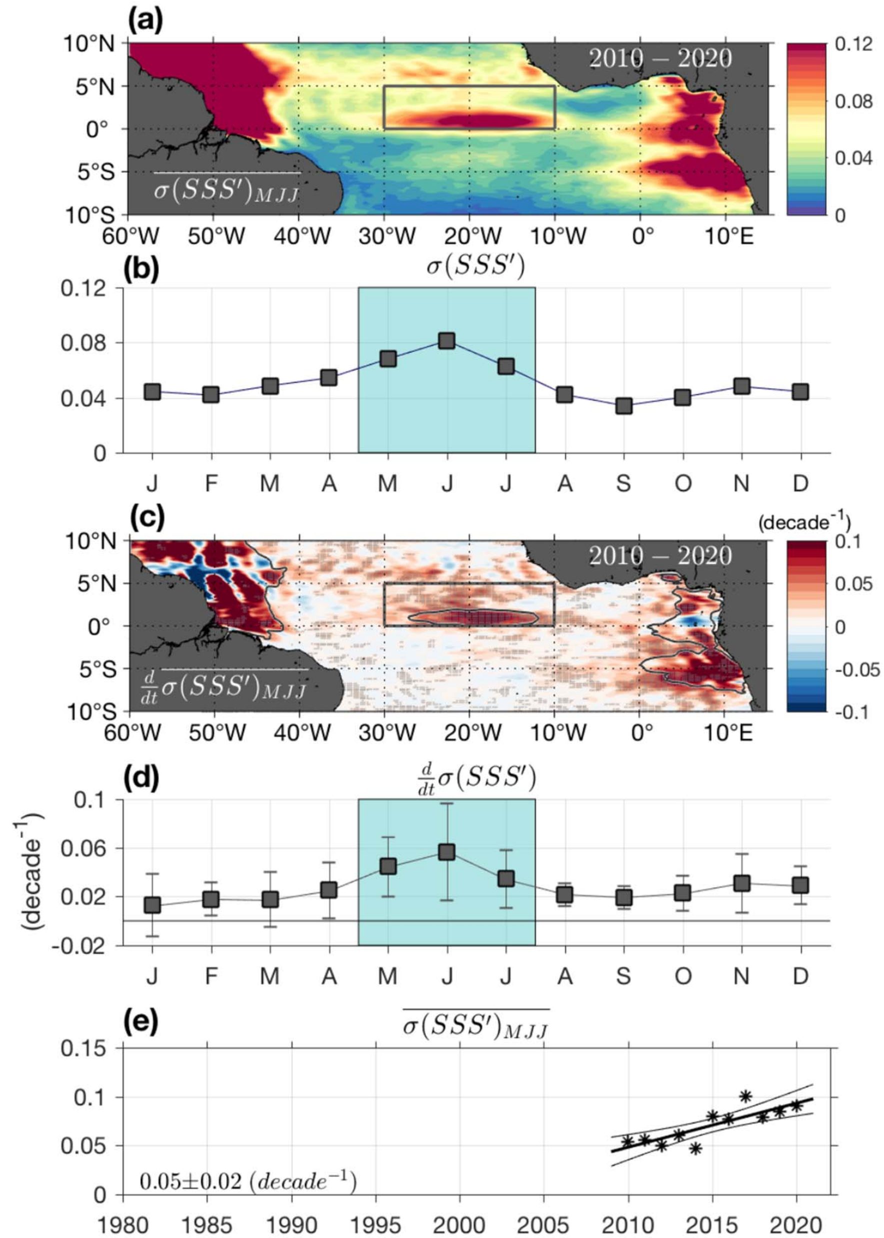

Figure S2. Standard deviation (***σ***) of bandpass filtered anomalies of sea surface salinity (SSS) for (a) the long-term mean seasonal ***σ*** in May to July, (b) spatial averages of monthly ***σ*** in the box and for the time period indicated in (a). (c) Decadal linear trend of intraseasonal variability of SSS during May to July. Significant trends are indicated by grey dots and one background TIW variability contour line from (a) is shown (thin black line). (d) Monthly SSS TIW variability trends spatially averaged over the box indicated in (c). (e) Time series of the yearly composite value for the spatial and temporal averages indicated in (c) and (d). Solid thin lines in (e) indicate the 95% confidence band. Primes indicate intraseasonal (20-50 day) and zonal (4-20°) band-pass filtered variables. Overbars indicate averages of the seasonal peak months highlighted in turquoise. Uncertainty estimates are based on a linear regression analysis (95% confidence interval).

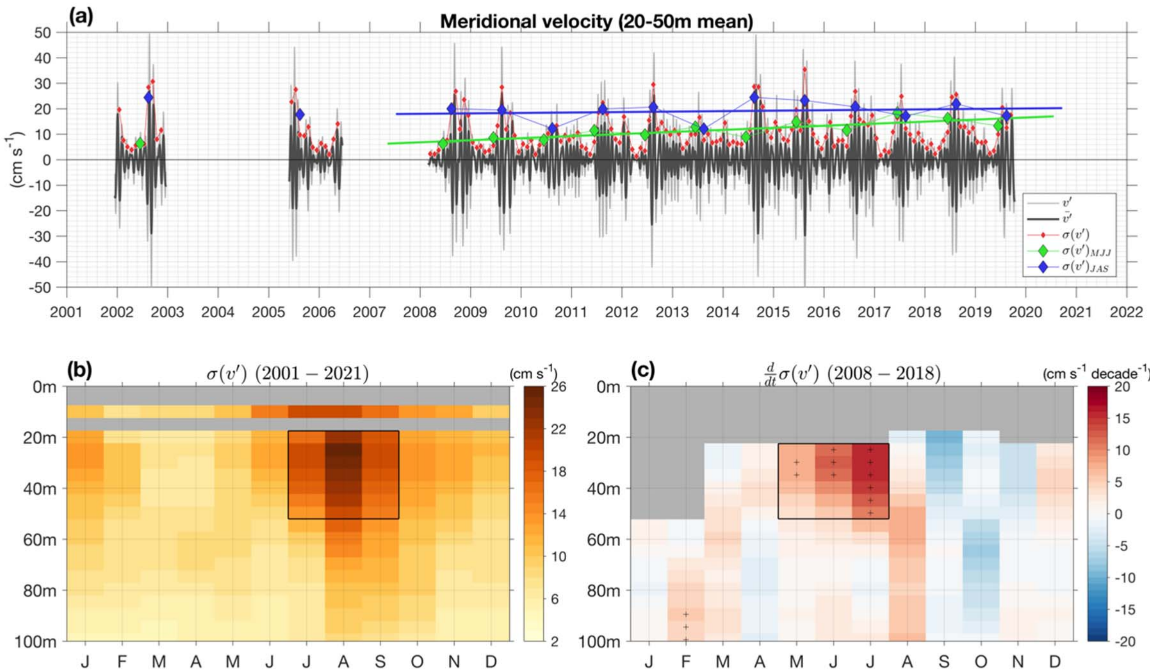

Figure S3. Subsurface intraseasonal meridional velocity from moored observations at 0°, 23°W. (a) Time series of filtered (20-50 day) meridional velocity ($\boldsymbol{v'}$), 30-day running mean ($\overline{\boldsymbol{v}'}$), and monthly standard deviation $\boldsymbol{\sigma}$ (red diamonds) as well as seasonal standard deviation averages for May to July (green diamonds) and July to September (blue diamonds). (b) Climatology of intraseasonal meridional velocity standard deviation. The black box indicates the depth range used for (a) and the annual maximum standard deviation from July to September used for the JAS composite in (a). Shallow measurements at 10 m from current meter data are only included in the climatology. (c) Decadal linear trend of intraseasonal meridional velocity standard deviation from 2008 to 2018. The black box indicates the decadal linear trend peak in May to July used for the MJJ composite in (a). Significant trend values (95% confidence interval) are indicated by black crosses.

Text S2: Covariance of zonal and meridional velocities from moored velocity observations at 0°, 23°W

The analysis of moored subsurface velocities at 0°, 23°W reveals a pronounced seasonal cycle in the covariance of zonal and meridional velocity fluctuations with maximum values from July to August ($u'v'$; Fig. S4a) that is not reproduced by the drifter-wind-altimetry synthesis product on the equator (Fig. 3). This suggests that positive barotropic energy conversion, meaning a generation site for TIWs, also occurs on the equator given the positive meridional gradient of zonal velocity close to the equator. Such a secondary band of barotropic energy conversion has been shown in the model study by *von Schuckmann et al. (2008)*.

Moored velocity observations further show that between 2008 to 2018 $u'v'$ has increased in July and August during this approximately decadal time period (Fig. S4b). This indicates that barotropic energy conversion has likely strengthened in the nSEC/EUC region near the equator, and this increase was not captured by the drifter-wind-altimetry-synthesis product (Fig. 3).

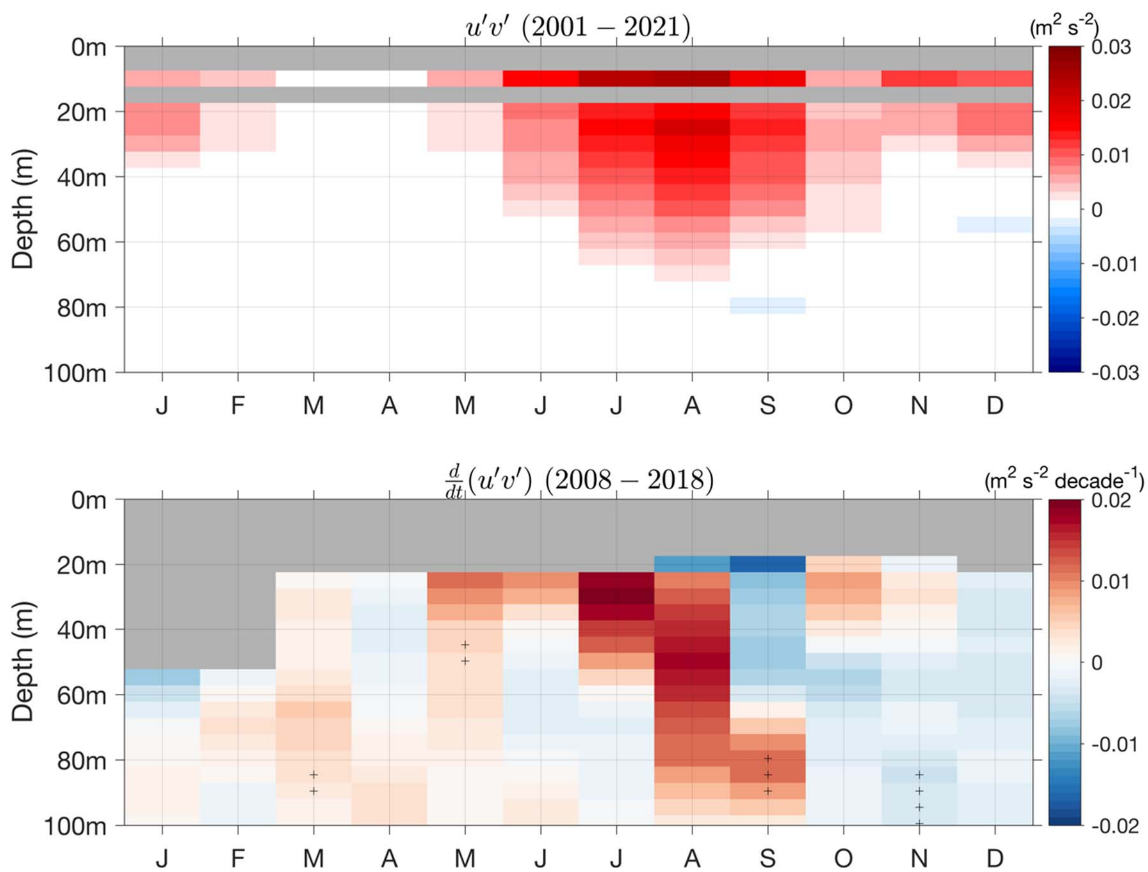

Figure S4. Covariance of horizontal velocity fluctuations ($\boldsymbol{u'v'}$) from moored velocity observations at 0°, 23°W. (a) Mean $\boldsymbol{u'v'}$ between 2001 to 2021. (b) Decadal linear trend of $\boldsymbol{u'v'}$ between 2008 to 2018. Significant trend values (95% confidence interval) are indicated by black crosses.

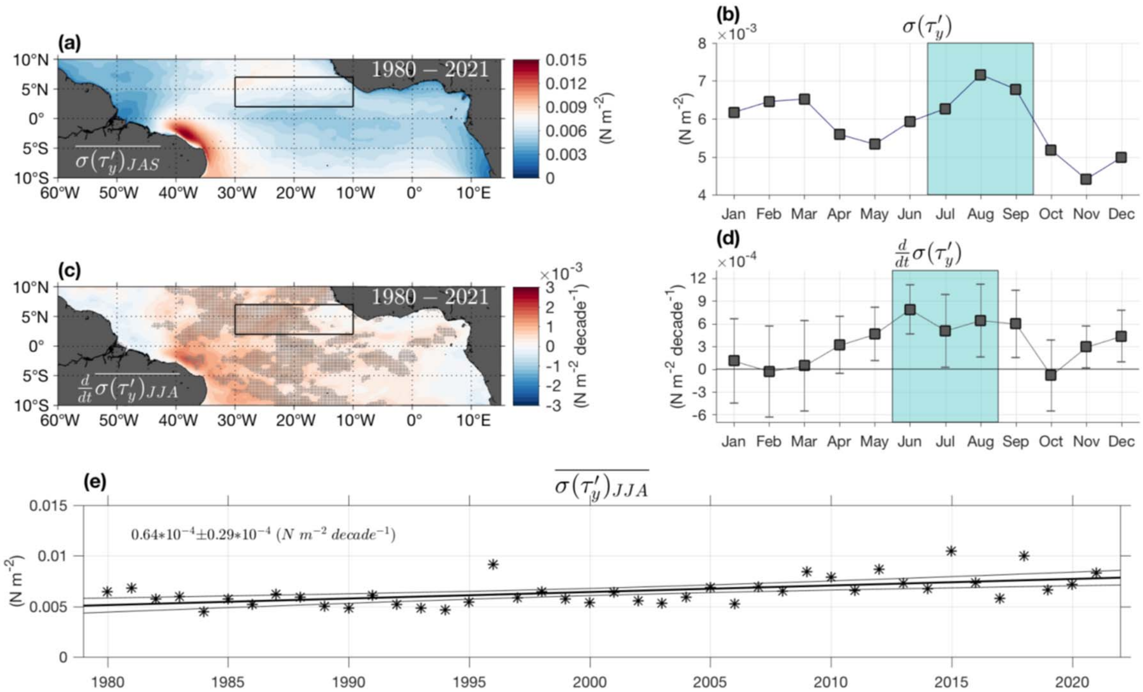

Figure S5. Standard deviation $\boldsymbol{\sigma}$ of intraseasonal (20-50 day) meridional wind stress for (a) the long-term mean during July to September, (b) in a climatological view for the region indicated in (a). (c) Decadal linear trend of $\boldsymbol{\sigma(\tau'_y)}$ during June to August. (d) Long-term monthly trends of $\boldsymbol{\sigma(\tau'_y)}$ for the region indicated in (a) and (c). Uncertainty estimates are based on a linear regression analysis (95% confidence interval). (e) Time series of the yearly composite value for the spatial and temporal averages indicated in (c) and (d). Solid thin lines in (e) indicate the 95% confidence band. Hourly 10-m wind speed data are provided by the European Centre for Medium-Range Weather Forecasts (ECMWF) ERA5 (*Hersbach et al., 2020*) from 1980 to 2021 and have been subsampled to daily fields.

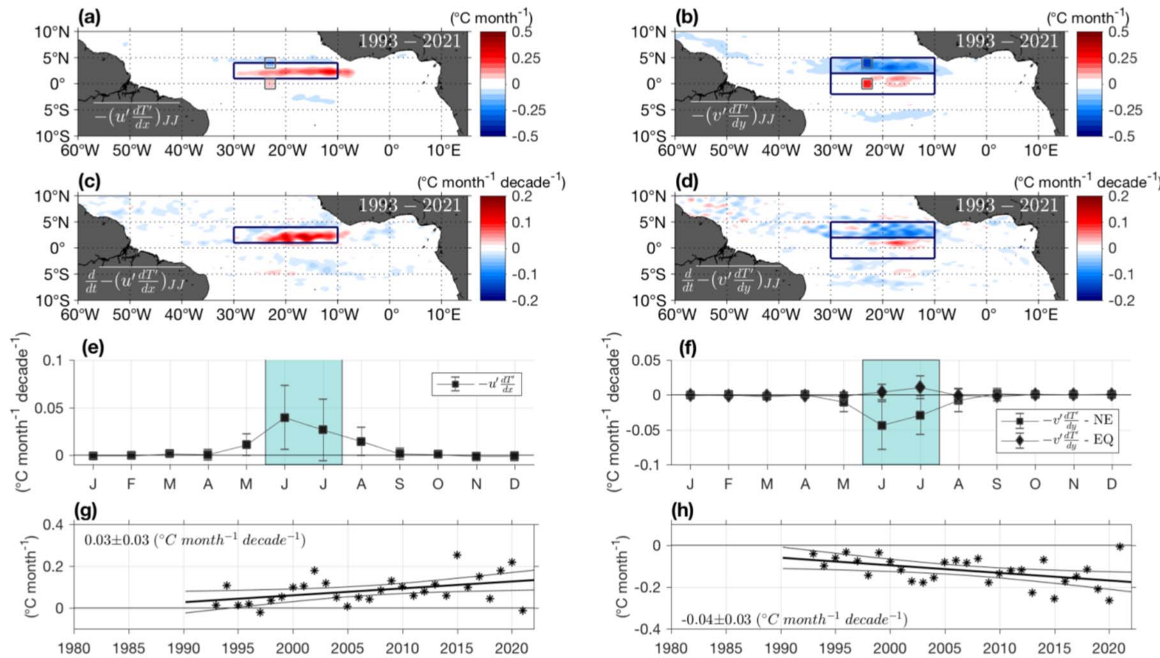

Figure S6. Zonal (left panels) and meridional (right panels) eddy temperature advection (ETA) in the tropical Atlantic due to Tropical Instability Waves at approximately 15 m depth. Primes indicate intraseasonal (20-50 day) and zonal (4°-20°) band-pass filtered variables. (a-b) Mean ETA from near-surface velocities and satellite SST averaged for June to July. Positive values indicate sea surface cooling, negative values indicate sea surface warming. Also shown in (a) and (b) is the mean ETA at the 23°W mooring sites on the equator and at 4°N using 10 m velocities and satellite SST. (c-d) Decadal linear trend of ETA for June to July. (e) Long-term monthly trends of zonal ETA for the box indicated in (c). (f) Long-term monthly trends of meridional ETA in a north equatorial (NE) box and an equatorial (EQ) box as indicated in (d). (g) Time series of the yearly composite value of zonal ETA for the spatial and temporal averages indicated in (c) and (e). (h) Time series of the yearly composite value of meridional ETA for the NE box during June to July. Solid thin lines in (g) and (h) indicate the 95% confidence band.

References

Bourlès, B., Araujo, M., McPhaden, M. J., Brandt, P., Foltz, G. R., Lumpkin, R., & Coauthors (2019), PIRATA: A Sustained Observing System for Tropical Atlantic Climate Research and Forecasting. *Earth and Space Science*, 6, 577-616. https://doi.org/10.1029/2018EA000428

Foltz, G. R., Brandt, P., Richter, I., Rodríguez-Fonseca, B., Hernandez, F., Dengler, M., & Coauthors (2019), The Tropical Atlantic Observing System. *Frontiers in Marine Science*, 6, 206. https://doi.org/10.3389/fmars.2019.00206

Hersbach, H., Bell, B., Berrisford, P., Hirahara, S., Horányi, A., Muñoz-Sabater, J., & Coauthors (2020), The ERA5 global reanalysis. *Quarterly Journal of the Royal Meteorological Society*, 146, 1999-2049. https://doi.org/10.1002/qj.3803

Lagerloef, G. S. E., Mitchum, G. T., Lukas, R. B., & Niiler, P. P. (1999), Tropical Pacific near-surface currents estimated from altimeter, wind, and drifter data. *Journal of Geophysical Research*, 104, 23313-23326. https://doi.org/10.1029/1999JC900197

Lumpkin, R., & Garzoli, S. L. (2011), Interannual to decadal changes in the western South Atlantic's surface circulation. *Journal of Geophysical Research*, 116, C01014. https://doi.org/10.1029/2010JC006285

Perez, R. C., Foltz, G. R., Lumpkin, R., & Schmid, C. (2019), Direct Measurements of Upper Ocean Horizontal Velocity and Vertical Shear in the Tropical North Atlantic at 4°N, 23°W. *Journal of Geophysical Research: Oceans*, 124, 4133-4151. https://doi.org/10.1029/2019JC015064

Tuchen, F. P., Brandt, P., Hahn, J., Hummels, R., Krahmann, G., Bourlès, B., & Coauthors (2022b), Two Decades of Full-Depth Current Velocity Observations From a Moored Observatory in the Central Equatorial Atlantic at 0˚N, 23˚W. *Frontiers in Marine Science*, 9:910979. https://doi.org/10.3389/fmars.2022.910979

von Schuckmann, K., Brandt, P., & Eden, C. (2008), Generation of tropical instability waves in the Atlantic Ocean. *Journal of Geophysical Research*, 113, C08034. https://doi.org/10.1029/2007JC004712